Multiaxial fatigue of water pipe grey cast iron

JOHN, Edward <http://orcid.org/0000-0002-8707-4197>, BOXALL, Joby <http://orcid.org/0000-0002-4681-6895>, COLLINS, Richard <http://orcid.org/0000-0001-5449-8535>, BOWMAN, Elisabeth <http://orcid.org/0000-0001-7868-6688> and SUSMEL, Luca <http://orcid.org/0000-0001-7753-9176>

International Journal of Fatigue 178 (2024) 108002

Contents lists available at ScienceDirect

International Journal of Fatigue

journal homepage: www.elsevier.com/locate/ijfatigue

Multiaxial fatigue of water pipe grey cast iron

Edward John, Joby Boxall, Richard Collins, Elisabeth Bowman, Luca Susmel *

Department of Civil and Structural Engineering, The University of Sheffield, Sheffield, UK

ARTICLE INFO

Keywords:
Multiaxial fatigue
High-cycle fatigue
Grey cast iron
Water pipe

ABSTRACT

Grey Cast Iron (GCI) water pipes are subjected to multiaxial, cyclic stresses caused by combinations of loads such as internal water pressure and road vehicle weight. However, the multiaxial fatigue performance of this material has not previously been characterised. To address this gap more than 45 fatigue tests, including some under non-proportional tension-torsion loading, were completed using a GCI material very similar to water pipe GCI. Of the four multiaxial fatigue criteria tested, the Smith-Watson-Topper (SWT) criterion provided the best predictions by a narrow margin, supporting the idea that a tensile cracking mode dominates the fatigue life of GCI.

1. Introduction

Pipes made of Grey Cast Iron (GCI) are common in many UK water distribution networks, and around the world, and are often identified as having high failure rates compared to other pipe materials [1,2]. The UK water industry has committed to halving leakage rates by 2050, compared to 2018 levels [3], but only replaces around 0.1 % of pipes per year [4]. As a result, old GCI pipes will not be completely removed from service in the foreseeable future. To help reduce leakage rates in a cost-effective way techniques must be developed which enable targeted replacement of old GCI water pipes [3].

GCI water pipes are vulnerable to corrosion which can result in the formation of localised pits or uniform wall loss [5,6]. The reduction in wall thickness caused by corrosion increases the stresses experienced by the pipe material and can lead to the formation of leaking cracks under service loading [7]. Years-to-leakage modelling for GCI water pipes based on predicting years to fatigue failure [8,9] has the potential to guide the selection of pipes for replacement. Corrosion of GCI water pipes has been extensively researched [5,10,11] but the fatigue response of the pipe material is less well understood and fundamental research is required to address this gap.

GCI pipes were used in new installations from the mid-1800s until the 1960s, but many still remain in service [1,12]. A defining feature of GCI is the graphite flake inclusions contained within its predominantly iron microstructure, as shown in Fig. 1. The extremely brittle tensile behaviour of GCI is attributed to these graphite flakes acting as internal defects [13,14]. GCI pipes were superseded in UK water networks by pipes made of Ductile Cast Iron (DCI), which is a stronger, less brittle cast iron [1]. The superior mechanical properties of DCI are in part due to the nodular morphology of the graphite found in DCI, instead of the graphite flakes found in GCI [13,15,16].

Brevis, Susmel and Boxall [8] predicted that millions of load cycles are required to cause a GCI pipe to crack, while Jiang *et al.* [9] predicted in the order of 10^4 load cycles would be required. Literature data for GCI indicate that the High-Cycle Fatigue (HCF) regime covers failures occurring between around 10^2 and 10^7 load cycles [9,17–20]. Therefore, for the water pipe application considered here the fatigue regime of interest is HCF. The relatively low stresses applied under HCF mean that for most materials linear elastic behaviour dominates and plastic strains become insignificant.

Smaller diameter GCI pipes can experience biaxial stress states; internal water pressure causes a pipe to experience stress acting around its circumference [21] and bending loads, such as vehicles and soil moisture response, cause stress acting in the pipe's axial direction [22,23]. These loads are also time variable with the potential to cycle tens or even hundreds of times per day [24–26]. As a result, models aiming to predict years to fatigue failure of GCI water pipes must be capable of predicting the multiaxial fatigue behaviour of GCI.

No data is currently available which describes the multiaxial fatigue behaviour of water pipe GCI, so it is not possible to select a multiaxial fatigue criterion for GCI water pipes. However, a large quantity of GCI uniaxial and rotating-bending fatigue data is available [9,17,19,20]. Additionally, Weinacht and Socie [18] reported tests of GCI specimens subject to strain-controlled torsional fatigue loads. Some multiaxial fatigue data is available for DCI; Tovo *et al.* [27] and Benedetti *et al.* [28] both performed in-phase and out-of-phase tension-torsion fatigue tests on DCI specimens. However, there is no literature available to suggest that GCI and DCI exhibit similar responses to multiaxial fatigue loading.

The work detailed in this paper aimed to identify a fatigue criterion

* Corresponding author.
E-mail address: l.susmel@sheffield.ac.uk (L. Susmel).

https://doi.org/10.1016/j.ijfatigue.2023.108002
Received 1 August 2023; Received in revised form 22 September 2023; Accepted 10 October 2023
Available online 13 October 2023

Nomenclature

A	MWCM criterion material constant
B	MWCM criterion material constant
b	Fatigue strength exponent
c	Fatigue ductility exponent
E	Elastic modulus
E_{RMS}	Logarithmic root mean square error
k	Negative inverse slope
k_τ	MWCM criterion negative inverse slope
m	MWCM criterion mean stress sensitivity index, a material property which ranges between 0 and 1
N_A	High-cycle reference cycles to failure
$N_{\mathrm{cal}(i)}$	Predicted cycles to failure for test i
$N_{\mathrm{exp}(i)}$	Experimentally observed cycles to failure for test i
N_f	Cycles to failure
n	Number of observations
P_s	Probability of survival
R	Load ratio, equal to $\sigma_{min}/\sigma_{max}$
T_{RMS}	Mean square error of prediction scatter
$T_{RMS,M}$	Mean square error of prediction scatter for uniaxial $R = 0.1$ loading
$T_{RMS,TT}$	Mean square error of prediction scatter for TTIP and TTOOP loading
$T\sigma$	Stress amplitude scatter
t	Time
α	MWCM criterion material constant
β	MWCM criterion material constant
δ	CS criterion angle in degrees between the weighted mean direction of maximum principal stress and the normal to the critical plane
$\varepsilon_f^{'}$	Fatigue ductility coefficient
$\varepsilon_{n,a}$	Normal strain amplitude on the critical plane
$\varepsilon_{X^{'}}$	Normal strain on an arbitrary material plane defined by the axes $X^{'}, Y^{'}, Z^{'}$ where $X^{'}$ is normal to the plane
κ	MMS criterion biaxiality ratio, equal to σ_2/σ_1 unless $\sigma_2/\sigma_1 > 0$ in which case $\kappa = 0$
λ	Biaxiality ratio, equal to σ_a/τ_a
ν	Poisson's ratio
ρ_{eff}	MWCM criterion effective stress ratio
σ_1, σ_2	Principal stresses
$\sigma_{A,P_S=10\%}$	10% probability of survival high cycle reference stress amplitude, determined at N_A cycles to failure
$\sigma_{A,P_S=50\%}$	50% probability of survival high cycle reference stress amplitude, determined at N_A cycles to failure
$\sigma_{A,P_S=90\%}$	90% probability of survival high cycle reference stress amplitude, determined at N_A cycles to failure
$\sigma_{A,R=-1}$	Uniaxial fully reversed reference stress amplitude, determined at N_A cycles to failure
$\sigma_{a,R=-1}$	Equivalent uniaxial fully reversed stress amplitude
$\sigma_f^{'}$	Fatigue strength coefficient
σ_a	Applied stress amplitude
σ_{max}	Maximum applied stress
σ_{min}	Minimum applied stress
$\sigma_{n,a}$	Normal stress amplitude on the critical plane
$\sigma_{n,m}$	Mean value of normal stress on the critical plane
$\sigma_{n,max}$	Maximum value of normal stress on the critical plane
σ_{UTS}	Ultimate tensile strength
$\sigma_{X^{'}}, \sigma_{Y^{'}}, \sigma_{Z^{'}}$	Stresses acting on an arbitrary material plane defined by the axes $X^{'}, Y^{'}, Z^{'}$ where $X^{'}$ is normal to the plane
$\sigma_{y,0.2\%}$	0.2% offset yield strength
$\tau_{A,R=-1}$	Torsional fully reversed reference stress amplitude, determined at N_A cycles to failure
$\tau_{A,Ref}$	MWCM criterion reference shear stress amplitude, determined at N_A cycles to failure
τ_a	Applied shear stress amplitude
$\tau_{cp,a}$	Resolved shear stress amplitude on the critical plane
ϕ	Phase shift of torsion loading relative to uniaxial loading

that is able to predict the multiaxial HCF response of water pipe GCI. Due to the lack of multiaxial fatigue data availabe for GCI, a programme of fatigue tests was carried out to provide the data needed to select a suitable criterion. To contextualise the choice of fatigue criteria investigated, the following section reviews the present understanding of crack formation and fatigue life prediction of GCI, and DCI to a lesser extent. Subsequent sections detail the experiments performed as part of this work, the results obtained, and the effectiveness of the various fatigue critera.

2. Fatigue criteria for GCI and DCI

As observed by Socie [29], when selecting a multiaxial fatigue criterion it is important to consider how cracks form and grow in the

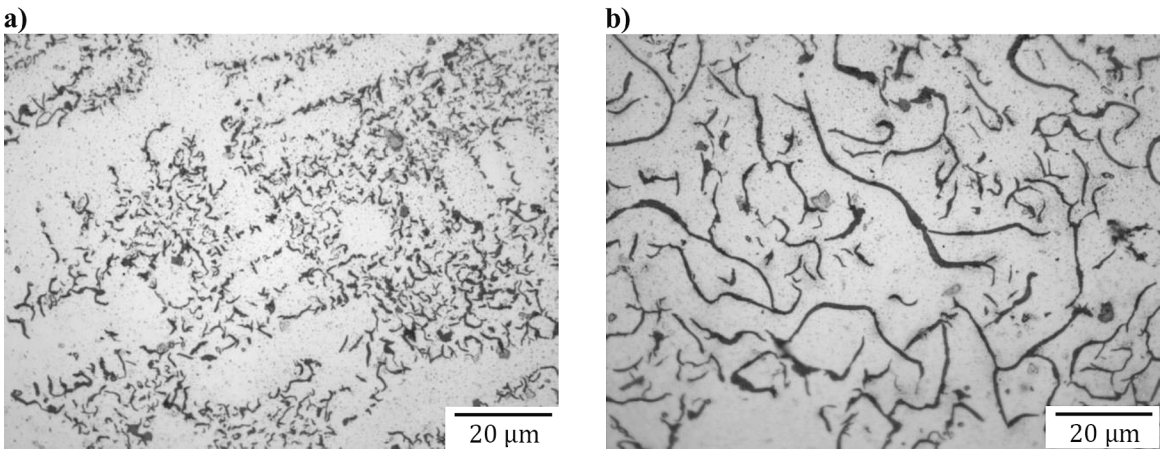

Fig. 1. X100 magnification images showing typical examples of the graphite microstructure of the bs416-2 pipe used to make the fatigue specimens.

material of interest. In metals, cracks typically nucleate in a single grain then grow to the size of several grains under a Mode II shearing mechanism (Stage I crack growth). After this, the crack switches to growing under a Mode I tensile mechanism (Stage II crack growth) until it is large enough to cause failure [30]. In some metals, 90% of the HCF life may be accounted for through fatigue crack initiation, in which case, modelling the Stage I process can be used to predict the fatigue life [31]. However, Weinacht & Socie [18] found that under torsional and uniaxial loading Stage II crack growth comprised 90–95% of the fatigue life of their GCI specimens. Marquis & Karjalainen-Roikonen [32] also observed the dominance of Stage II crack growth for DCI. This is potentially because the defects found in GCI and DCI create stress concentrations that accelerate crack initiation and Stage I growth [33,34].

Critical plane multiaxial fatigue criteria typically aim to model the fatigue cracking process described above using some function of the stress and/or strain quantities that are thought to drive fatigue crack initiation and/or growth. These stress and/or strain quantities are taken on a 'critical plane' that is defined by the criteria and is often the plane on which the fatigue crack is expected to initiate and/or grow. The resultant value of the function is then used to compare different load histories and hence make fatigue life predictions.

Weinacht & Socie [18] successfully applied the Smith-Watson-Topper (SWT) fatigue criterion using a critical plane approach to predict the response of GCI specimens to torsional loading, where the critical plane is that which experiences the maximum normal strain amplitude. Fash & Socie [17] found that the SWT criterion was also able to account for the mean stress effect for GCI in the HCF regime. For DCI, Marquis & Karjalainen-Roikonen [32] modified a maximum normal stress critical plane model initially developed by Marquis and Socie [35] and based on the Goodman mean stress correction factor. This model is referred to hereafter as the Modified Marquis-Socie (MMS) criterion. The MMS criterion was found effective at predicting torsional and equibiaxial fatigue limits. Benedetti *et al.* [28] applied a range of critical plane criteria to smooth and notched DCI, finding the Modified Smith Watson Topper (MSWT) and Carpinteri–Spagnoli (CS) criteria to be most effective; both criteria are normal stress, or strain, criteria. The shear stress-based Modified Wöhler Curve Method (MWCM) and shear stress and strain-based Fatemi-Socie (FS) criteria were also assessed but were found to be less effective. As discussed in Section 1, the fatigue regime of interest for water pipes is HCF which made stress-based fatigue criteria more appropriate for consideration [36]. Therefore, the effectiveness of the three stress-based criteria (MMS, CS and MWCM) were assessed in this study. Due to its successful prior applications to GCI, the SWT criterion was also assessed, but in a stress-based form. These four criteria are introduced below.

The SWT criterion was proposed by Smith, Topper, and Watson [37] and is expressed for multiaxial fatigue assessment as:

$$\sigma_{n,max}\varepsilon_{n,a} = \frac{\sigma_f^{'2}}{E}(2N_f)^{2b} + \sigma_f^{'}\varepsilon_f^{'}(2N_f)^{b+c} \tag{1}$$

where: $\sigma_{n,max}$ is the maximum value of normal stress on the critical plane; ε is the normal strain amplitude on the critical plane; E is the material's elastic modulus; $\sigma_f^{'}$ is the fatigue strength coefficient; $\varepsilon_f^{'}$ is the fatigue ductility coefficient; b is the fatigue strength exponent; c is the fatigue ductility exponent; and N_f is the number of loading cycles to failure. The critical plane is that which experiences the greatest normal strain amplitude [29]. For linear elastic behaviour equation (1) equates to the equivalent fully reversed uniaxial stress amplitude [38]:

$$\sigma_{a,R=-1} = \sqrt{\sigma_{n,max}E\varepsilon_{n,a}} \tag{2}$$

where $\sigma_{a,R=-1}$ is the equivalent uniaxial fully reversed stress amplitude, given $R = \sigma_{min}/\sigma_{max}$. To apply the SWT criterion using a stress-based approach the normal strain on an aribtrary material plane, $\varepsilon_{X'}$, multiplied by the material elastic modulus, may be calculated from the plane's stresses at any point during a load history using Hooke's law:

$$E\varepsilon_{X'}(t) = \sigma_{X'}(t) - \nu[\sigma_{Y'}(t) - \sigma_{Z'}(t)] \tag{3}$$

where: $\sigma_{X'}$, $\sigma_{Y'}$ and $\sigma_{Z'}$ are the stresses acting on an arbitrary material plane defined by the axes $X^{'}, Y^{'}, Z^{'}$ where $X^{'}$ is normal to the plane; ν is the material's Poisson ratio; and t is time. $E\varepsilon_{n,a}$ is calculated from $E\varepsilon_{X'}(t)$ for each plane, and the critical plane is that which features the maximum value of $E\varepsilon_{n,a}$. Cycles to failure are predicted using equation (4):

$$N_f = N_A\left(\frac{\sigma_{A,R=-1}}{\sigma_{a,R=-1}}\right)^k \tag{4}$$

where: N_A is the high-cycle reference cycles to failure; $\sigma_{A,R=-1}$ is the uniaxial fully reversed reference stress amplitude, determined at N_A cycles to failure; and k is the uniaxial fully reversed negative inverse slope.

The MMS critierion is expressed as [32]:

$$\sigma_{a,R=-1} = \left[\frac{1}{(1-0.25\kappa)} - \frac{2\sigma_{n,m}}{\sigma_{UTS}+\sigma_{y,0.2\%}}\right]^{-1}\sigma_{n,a} \tag{5}$$

where: $\sigma_{n,a}$ is the normal stress amplitude on the critical plane, and the critical plane is that experiencing the maximum value of $\sigma_{n,a}$; $\sigma_{n,m}$ is the mean stress on the critical plane; $\kappa = \sigma_2/\sigma_1$ unless $\sigma_2/\sigma_1 > 0$ in which case $\kappa = 0$, where σ_1 and σ_2 are the principal stresses on the critical plane; σ_{UTS} is the material ultimate tensile strength; and $\sigma_{y,0.2\%}$ is the material 0.2% offset yield strength. The number of cycles to failure is then predicted using equation (4).

Like equation (5), the CS criterion includes a Goodman-type combination of the mean and amplitude of the normal stress acting on the critical plane. For the CS criterion the critical plane angle is defined by [39]:

$$\delta = 45\frac{3}{2}\left[1 - \left(\frac{\tau_{A,R=-1}}{\sigma_{A,R=-1}}\right)^2\right] \tag{6}$$

where: δ is the angle in degrees between the weighted mean direction of maximum principal stress and the normal to the critical plane; and $\tau_{A,R=-1}$ is the torsional fully reversed reference stress amplitude. For plane stress the weighted mean direction of maximum principal stress can be simplified to the direction experiencing the maximum principal stress [40]. The equivalent uniaxial fully reversed stress amplitude is then calculated on the critical plane using equation (7) [40]:

$$\sigma_{a,R=-1} = \sqrt{\left[\sigma_{n,a} + \sigma_{n,m}\left(\frac{\sigma_{A,R=-1}}{\sigma_{UTS}}\right)\right]^2 + \left(\frac{\sigma_{A,R=-1}}{\tau_{A,R=-1}}\right)^2\tau_{cp,a}^2} \tag{7}$$

where $\tau_{cp,a}$ is the shear stress amplitude on the critical plane. Cycles to failure is then determined using equation (4).

While the MWCM is primarily a shear-stress criterion, the impacts of stress normal to the critical plane are accounted for in the MWCM through the critical plane stress ratio, ρ_{eff} [41]:

$$\rho_{eff} = \frac{m\sigma_{n,m} + \sigma_{n,a}}{\tau_{cp,a}} \tag{8}$$

where m is the mean stress sensitivity index, a material property which ranges between 0 and 1. The high-cycle fatigue curve of a material can be characterised by a reference stress amplitude, at a specified number of cycles to failure, and the slope of the fatigue curve when plotted on log-log axis. The MWCM considers both these parameters to be linear functions of ρ_{eff} which are expressed as follows [41]:

$$\tau_{A,Ref}(\rho_{eff}) = \alpha\rho_{eff} + \beta \tag{9}$$

$$k_\tau(\rho_{eff}) = A\rho_{eff} + B \tag{10}$$

where $A, B, \alpha,$ and β are material constants determined from the fully reversed uniaxial and fully reversed torsional fatigue curves. To determine m a fatigue curve for uniaxial loading with a mean stress is also required. Cycles to failure are calculated using a shear stress version of equation (4) where $\sigma_{A,R=-1}$ is replaced by $\tau_{A,Ref}(\rho_{eff})$, k is replaced by $k_\tau(\rho_{eff})$, and $\sigma_{a,R=-1}$ is replaced by $\tau_{cp,a}$.

3. Experiments

The experiments conducted for this study aimed to generate the data required to calibrate the four fatigue criteria selected for assessment in Section 2 and test the ability of these criteria to predict the multiaxial fatigue behaviour of water pipe GCI. An additional aspect of these experiments was to investigate the cracking behaviour demonstrated by the water pipe GCI under different load types to build up a picture of how this material fails under HCF.

GCI water pipes are no longer manufactured and exhumed water pipes are often heavily corroded [42,43]. It is also difficult to obtain large amounts of metallurgically similar pipe material and produce torsional specimens from pipe walls. To overcome these challenges, fatigue specimens were produced from 16 new BS416-2 [44] soil pipes sourced from the same foundry (Hargreaves Foundry, Halifax, UK). These pipes have very similar graphitic microstructures and tensile stress-strain properties to water pipes [45]. The graphite flake sizes observed in these pipes ranged from <10 μm to around 80 μm (see Fig. 1). Additional 'dog-bone' specimen tensile tests were performed to characterise the material comprising the inside half of the pipe's wall, the results of which are shown in Table 1.

To enable tension-torsion testing the thin-walled tube specimen design, shown by Fig. 2, was developed. The specimens were produced by turning a gauge section into a length of DN50 BS 416-2 pipe. The wall thickness of the pipe was reduced by approximately 50% to produce the gauge section with a wall thickness of around 1.9 mm, although the inside diameter of the pipes did vary somewhat due to the casting process used. The spin-casting process used to manufacture the BS416-2 pipes meant that the roughness of the un-machined inside surface did not vary significantly between specimens. Average roughness values for the inside surface fell between 5 and 10 μm.

As shown by Table 2, the uniaxial $R = -1$, uniaxial $R = 0.1$, and torsional $R = -1$ fatigue curves were required for calibration purposes. To characterise these curves with sufficient certainty, five stress levels were tested with two repeats per stress level. Multiaxial stress histories can either be proportional, where the principal stress axes do not change with time, or non-proportional, where the principal stress axes do vary with time [30]. Non-proportional loading represents a more challenging condition for fatigue criteria to predict due to the potential for non-proportional hardening and because the principal directions rotate during the loading cycle [36]. To establish the effectiveness of each criterion under proportional and non-proportional multiaxial loading one of each load type was tested; these were tension-torsion in-phase (TTIP) loading and tension-torsion 90° out-of-phase (TTOOP) loading, respectively. For these multiaxial loadings the aim was to generate some data points across a range of stress amplitudes to compare against the model predictions, not to characterise the curves fully, so three stress levels were tested with five specimens. Therefore, around forty fatigue tests were conducted for the testing programme.

Table 1
Average monotonic tensile properties of the material used to produce the fatigue specimens, determined from "dog-bone" specimen tests.

Property	Average value
Elastic modulus (GPa)	74.9
Poisson ratio	0.26
Ultimate tensile strength (MPa)	203
Ultimate tensile strain (με)	5360

Fatigue testing was conducted using a Schenck servo-hydraulic rig (axial load capacity 400 kN, torsional load capacity 1 kNm) controlled by a MOOG SmarTEST ONE. Grips capable of holding 58 mm diameter tubular specimens were not available, so RCK80-60x77 Cross and Morse shaft clamps were used in combination with custom hubs that were bolted to the rig actuators.

The average stiffness during the two trial tests was calculated from the applied load and extensometer measurements. Specimen separation occurred very suddenly with no indicative preceding stiffness drop. As a result, specimen separation was used as the failure condition for all following fatigue tests.

Specimens with visible casting defects on the fracture surface were excluded from the subsequent statistical analysis to ensure that the unnotched fatigue characteristics of the material were captured. The ratio of shear to normal stress amplitude was 1 for all tension-torsion tests as uniaxial and torsional fatigue were found to be approximately equally damaging when applied independently. $2x10^6$ cycles was used as the runout definition for all tests.

4. Results

The cycles to failure vs applied stress amplitude for each fatigue test are plotted in Fig. 3 and Fig. 4. The exact intended stress level was rarely achieved in practice because the internal diameter of the specimen at the gauge section varied slightly between specimens and was difficult to measure accurately before testing. The stress levels plotted and used for subsequent analysis were determined from the more accurate wall thickness measurements of the fracture surface after the test, hence the lack of clear stress levels in many of the data sets. Due to the highly brittle nature of the material investigated no discernible necking of the tensile specimens was observed, meaning these fracture surface measurements were representative of the specimens' pre-test dimensions.

According to the defect criteria explained in the previous section, a total of ten test results were classed as coming from defective specimens and were not included in subsequent analyses. These results are marked on the relevant fatigue curves for reference.

The least squares method was used to estimate the relationship between stress amplitude and cycles to failure according to ASTM E739-10 [46] for each loading type. The least squares relationships are plotted as the 50% probability of survival curves in Fig. 3 and Fig. 4. The 50% probability of survival high cycle reference stress amplitude at 10^6 cycles, $\sigma_{A,P_S=50\%}$, and negative inverse slope, k, are provided in Table 3. The 10% and 90% probability of survival scatter bands were also calculated at a 95% confidence level for the uniaxial $R = -1$, uniaxial $R = 0.1$, and torsional $R = -1$ loading curves according to ASTM STP91 [47]. Scatter bands were not calculated for TTIP and TTOOP loading because the small number of data points for these load types would have made the resultant scatter bands non-representative. To quantify the degree of scattering observed $T\sigma$ values were calculated from the scatter bands. $T\sigma$ is a measure of the observed scattering of the fatigue data [48] and is the ratio of the 10% and 90% stress amplitudes at 10^6 cycles:

$$T\sigma = \frac{\sigma_{A,P_S=10\%}}{\sigma_{A,P_S=90\%}} \tag{11}$$

For comparison purposes, several sets of GCI and DCI fatigue data from the literature were also processed using the same method applied to the fatigue data generated for this study.

For the uniaxial loading results shown in Fig. 3, the $R = 0.1$ data all fell outside the $R = -1$ scatter bands indicating the material was sensitive to mean stress. Interestingly, all the data points for defective specimens under a load ratio of $R = -1$ fell within the scatter bands determined using the non-defective data, but for $R = 0.1$ loading the effect of defects was more pronounced. The tension-torsion (TT) results in Fig. 4 show that the addition of a tensile load had a damaging effect relative to pure torsion. The different phasing of the TT loads appears to

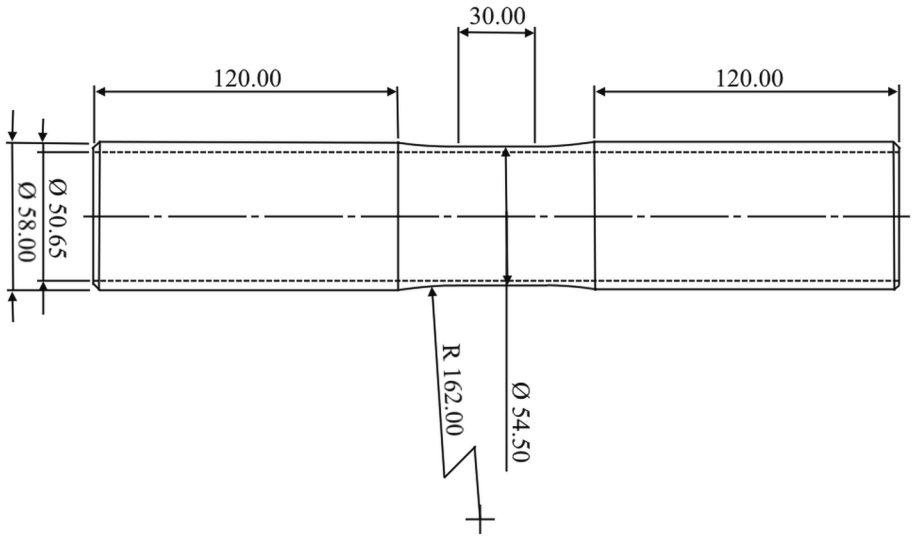

Fig. 2. Fatigue specimen geometry.

Table 2
Required calibration fatigue curves for each fatigue criteria and load types tested.

	Uniaxial $R = -1$	Uniaxial $R = 0.1$	Torsional $R = -1$	Tension-torsion $R = -1$ $\phi = 0^{\circ}$ $\lambda = 1$	Tension-torsion $R = -1$ $\phi = 90^{\circ}$ $\lambda = 1$
SWT	Calibration	Test	Test	Test	Test
MMS	Calibration	Test	Test	Test	Test
CS	Calibration	Test	Calibration	Test	Test
MWCM	Calibration	Calibration	Calibration	Test	Test

have had no clear effect. For all loading types few failures occurred after about $2x10^5$ cycles indicating the knee points of the fatigue curves may lie close to this value.

The angle of the fracture surface relative to the specimen longitudinal axis appeared to vary depending on the loading type. For uniaxial loading, regardless of the mean stress, the fracture surface was always close to 90° from the specimen's longitudinal axis (Fig. 5a), which is also the inclination of the maximum normal stress amplitude plane for this loading. For both tension and TTIP loading the fracture surface angles were approximately 45° (Fig. 5b), although individual fracture surfaces typically featured a range of inclinations that deviated from this value by up to 15°. The inclination of the maximum normal stress amplitude planes for tension and TTIP loading are 45° and 58°, respectively. The fracture surface inclination of each TTOOP specimen ranged between

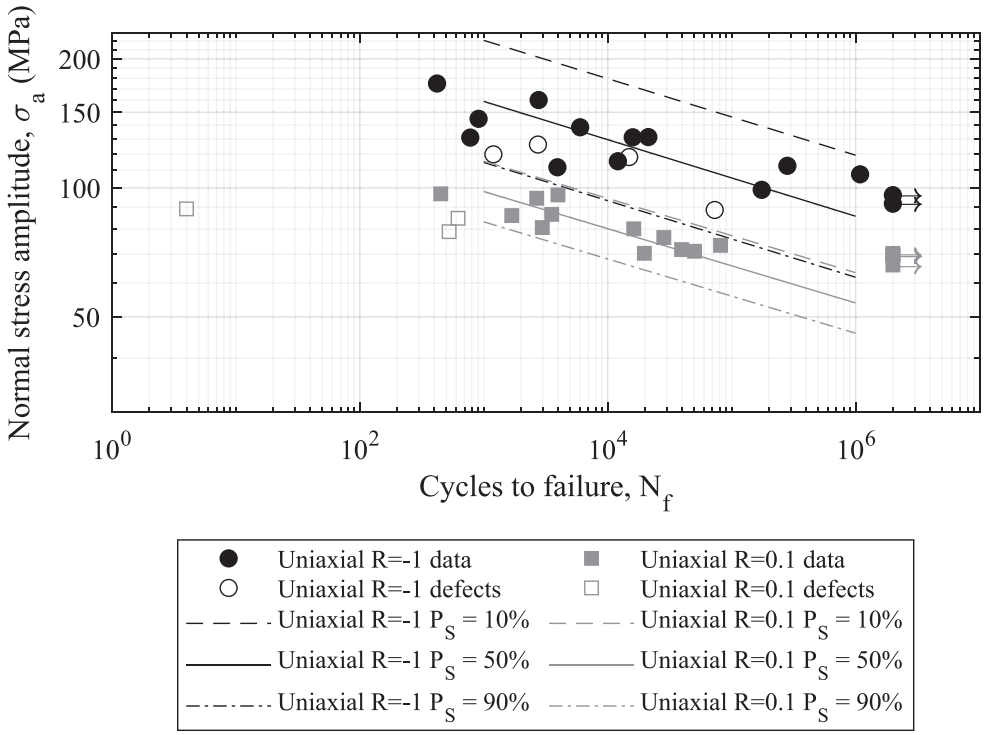

Fig. 3. Fatigue data and fitted curves for uniaxial loading.

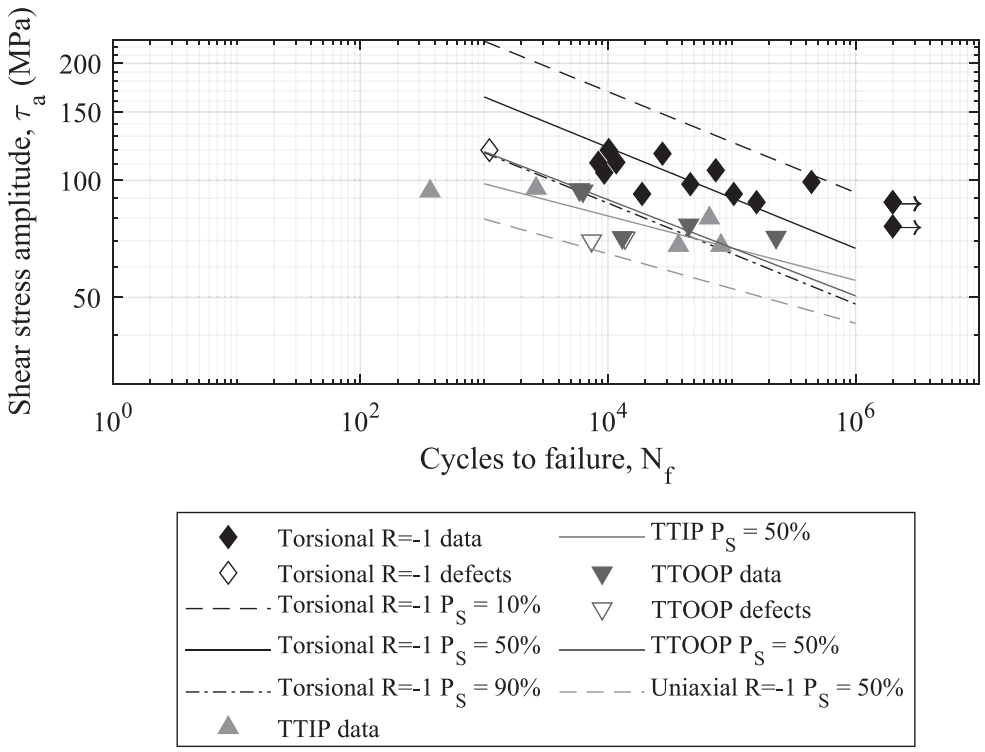

Fig. 4. Fatigue data for torsion and tension-torsion loading. Uniaxial $R = -1$ $P_S = 50\%$ line included for reference.

Table 3
Fatigue curves for GCI and DCI from the present work and literature. All data sets were processed using the same method. $\sigma_{A,P_S=50\%}$ was evaluated at 10^6 cycles for every data set and is given in terms of normal stress for all loading types.

Load type	Source	Material	σ_{UTS}(MPa)	n	R	k	$\sigma_{A,P_S=50\%}$(MPa)	$\frac{\sigma_{A,P_S=50\%}}{\sigma_{UTS}}$	T_σ
Axial	Present work BS416-2 pipe	GCI, spun-cast pipe	203	12	−1	11.5	85.8	0.44	1.9
	Tovo *et al.* [27]	DCI	460	8	−1	12.7	182.3	0.40	1.4
	Benedetti *et al.* [28]	DCI	458	12	−1	7.3	181. 6	0.40	1.3
Rotating bending	Kommers [19], Series C	GCI, spun-cast pipe	209	14	−1	8.4	94.7	0.45	1.4
	Kommers [19], Series G	GCI, sand-mould casting	245	17	−1	6.4	109.6	0.45	1.9
Axial with mean stress	Present work BS416-2 pipe	GCI, spun-cast pipe	203	12	0.1	10.5	53.9	0.26	1.5
	Jiang *et al.* [9], Pipe 1	GCI, pit-cast pipe	104	12	0.1	12.9	24.2	0.23	1.3
	Jiang *et al.* [9], Pipe 3	GCI, spun-cast pipe	173	8	0.1	17.5	47.6	0.28	1.3
	Jiang *et al.* [9], Pipe 5	GCI, spun-cast pipe	214	11	0.1	16.0	55.1	0.26	1.3
	Tovo *et al.* [27]	DCI	460	6	0	10.8	103.0	0.22	1.5
Torsion	Present work BS416-2 pipe	GCI, spun-cast pipe	203	11	−1	7.7	66.9	0.32	1.9
	Tovo *et al.* [27]	DCI	460	10	−1	9.9	177.5	0.39	1.2
	Benedetti *et al.* [28]	DCI	458	10	−1	8.2	187.1	0.41	1.3
Tension-torsion in-phase	Present work BS416-2 pipe	GCI, spun-cast pipe	203	5	−1	12.1	55.4	0.27	–
	Tovo *et al.* [27]	DCI	460	10	−1	7.5	112.1	0.24	1.2
	Benedetti *et al.* [28]	DCI	458	12	−1	6.4	110.4	0.24	1.3
Tension-torsion 90° out-of-phase	Present work BS416-2 pipe	GCI, spun-cast pipe	203	5	−1	8.1	50.1	0.25	–
	Tovo *et al.* [27]	DCI	460	6	−1	8.2	125.8	0.27	1.4
	Benedetti *et al.* [28]	DCI	458	10	−1	12.8	144.5	0.32	1.2

about 10° and 80° (Fig. 5c). For TTOOP loading the plane experiencing the maximum normal stress amplitude lies at an inclination of 55°. From the above it can be seen that for each load type, expect TTOOP, the fracture surface inclination matched the inclination of maximum normal stress amplitude plane quite closely, indicating that Mode I crack propagation was dominant at a macroscopic level for these loadings. For TTOOP loading, the principal stress axes likely rotated during the crack propagation process, resulting in the wide range of fracture surface inclinations observed.

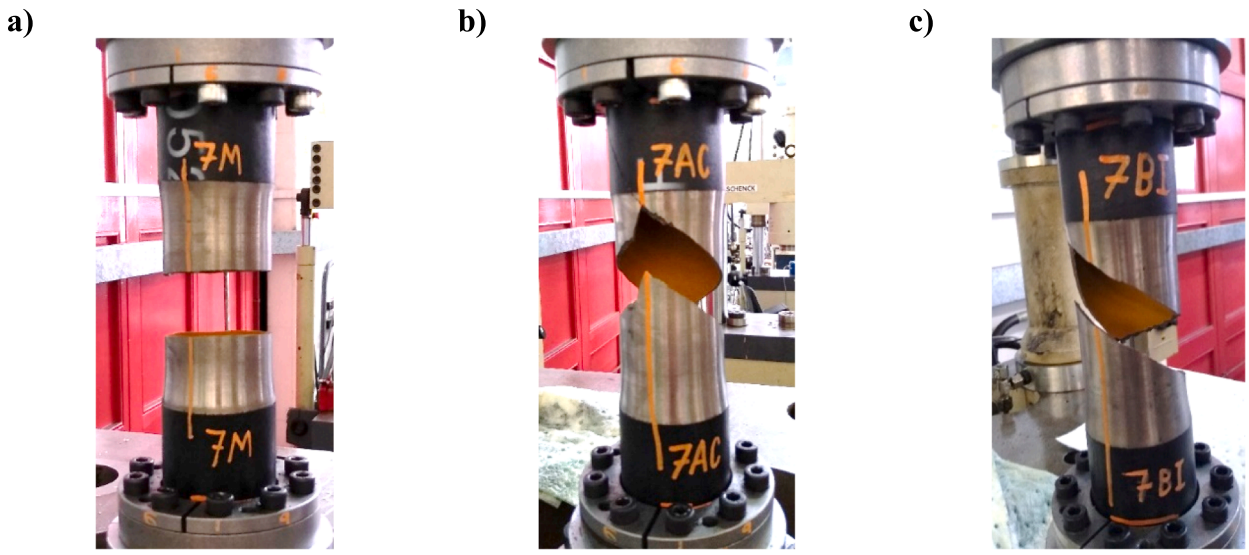

Fig. 5. Examples of failed specimens tested under a) uniaxial loading, b) torsional loading, and c) out-of-phase tension-torsion loading.

5. Estimates

Due to the relatively simple stress histories applied, $\tau_{cp,a}$ was calculated for the CS and MWCM criteria using the longest chord method [41]. The CS and MWCM fatigue criteria were calibrated as described in Section 2 using the fatigue data sets shown by Table 2. For the CS criterion the off-angle, δ, was found to be 26.5°. For calibration of the MWCM criterion, Susmel [49] recommended that in most cases a limit be imposed on the maximum value of ρ_{eff} to account for observations that above a certain level, increasing ρ_{eff} no longer had the expected effect on $\tau_{A,Ref}$. However, for the BS416-2 material the ρ_{eff} calculated for uniaxial $R = 0.1$ loading was greater than the recommended limit. Therefore, no limits were placed on the value of ρ_{eff} when applying the MWCM to this material. The calibration parameters determined for the MWCM are provided in Table 4. For the SWT and MMS criteria, the uniaxial 50% probability of survival curve parameters were used in equation (4) to make cycles to failure predictions.

The SWT, MMS, CS, and MWCM fatigue criteria were used to predict the cycles to failure of each data point from Fig. 3 and Fig. 4, excluding those classed as defects. The fatigue criteria predicted cycles to failure are plotted against the measured cycles to failure in Fig. 6 for all load types. The effectiveness of each fatigue criterion was quantified using the mean square error quantity, T_{RMS}, given by Walat and Łagoda [50] as:

$$E_{RMS} = \sqrt{\frac{\sum_{i=1}^{n}\left[\left(\log\frac{N_{\exp(i)}}{N_{\mathrm{cal}(i)}}\right)^2\right]}{n}} \tag{12}$$

$$T_{RMS} = 10^{E_{RMS}} \tag{13}$$

where: E_{RMS} is the logarithmic root mean square error; n is the number of observations; $N_{\exp(i)}$ is the experimentally observed cycles to failure for test i; and $N_{\mathrm{cal}(i)}$ is the predicted cycles to failure for test i.

The two TT load types (TTIP and TTOOP) were the only data not used to calibrate any fatigue criteria, while the uniaxial $R = 0.1$ data was only used to calibrate the MWCM. Therefore, to compare the effectiveness of the fatigue criteria, T_{RMS} values were calculated for the TT loadings for each fatigue criterion ($T_{RMS,TT}$) and also for uniaxial $R = 0.1$ loading ($T_{RMS,M}$), but for only the SWT, MMS and CS criteria. These T_{RMS} values are given in Fig. 6.

Table 4
Parameters determined for the MWCM.

Parameter	Value
α	–23.8
β	66.9
A	3.49
B	7.70
m	0.55

6. Discussion

In this work, new BS416-2 soil pipes were used as an alternative to exhumed GCI water pipes for fatigue testing, justified by the fact their tensile properties and graphite microstructure matched closely. Before moving on to discuss other aspects of the results it is important to first determine whether the BS416-2 pipe material is also representative of water pipe GCI from a fatigue perspective by comparing the measured fatigue properties of the BS416-2 pipes with the available literature data from uniaxial fatigue tests of actual GCI water pipe material.

From Table 3, the axial $R = -1$ and axial $R = 0.1$ high-cycle reference amplitudes ($\sigma_{A,P_S=50\%}$) taken at 10^6 cycles for the BS416-2 and literature GCI pipes match closely when scaled by UTS. Therefore, both the high cycle uniaxial fatigue strength and the magnitude of the mean stress effect observed for the BS416-2 pipe material is consistent with that of water pipe GCI. The BS416-2 pipe $R = -1$ and $R = 0.1$ negative inverse slopes of 11.5 and 10.5, respectively, fall between the values reported by Jiang et al. [9] for $R = 0.1$ loading (12.9 to 17.5) and Kommers' [19] Series C for $R = -1$ loading (8.4). Hence, the uniaxial loading 50% probability of survival curves of the BS416-2 pipe material were considered representative of GCI water pipes due to their high similarity.

Scattering of the four literature GCI water pipe data sets were characterised by T_σ of 1.3 or 1.4, less than the value of 1.9 calculated for the BS416-2 pipe under fully reversed axial loading. On the other hand, the T_σ value for the BS416-2 pipe under axial loading with a mean stress was similar to the literature data. The scatter of Kommers' [19] Series G GCI was also characterised by a T_σ of 1.9 indicating that this T_σ value is not unreasonable for GCI.

Literature multiaxial fatigue data for GCI is not available, however, some multiaxial fatigue data is available for DCI. Comparison of the multiaxial fatigue responses of GCI and DCI has therefore not previously been possible and is interesting from a water pipe perspective as DCI has also been used as a pipe material. Multiaxial fatigue data for DCI from

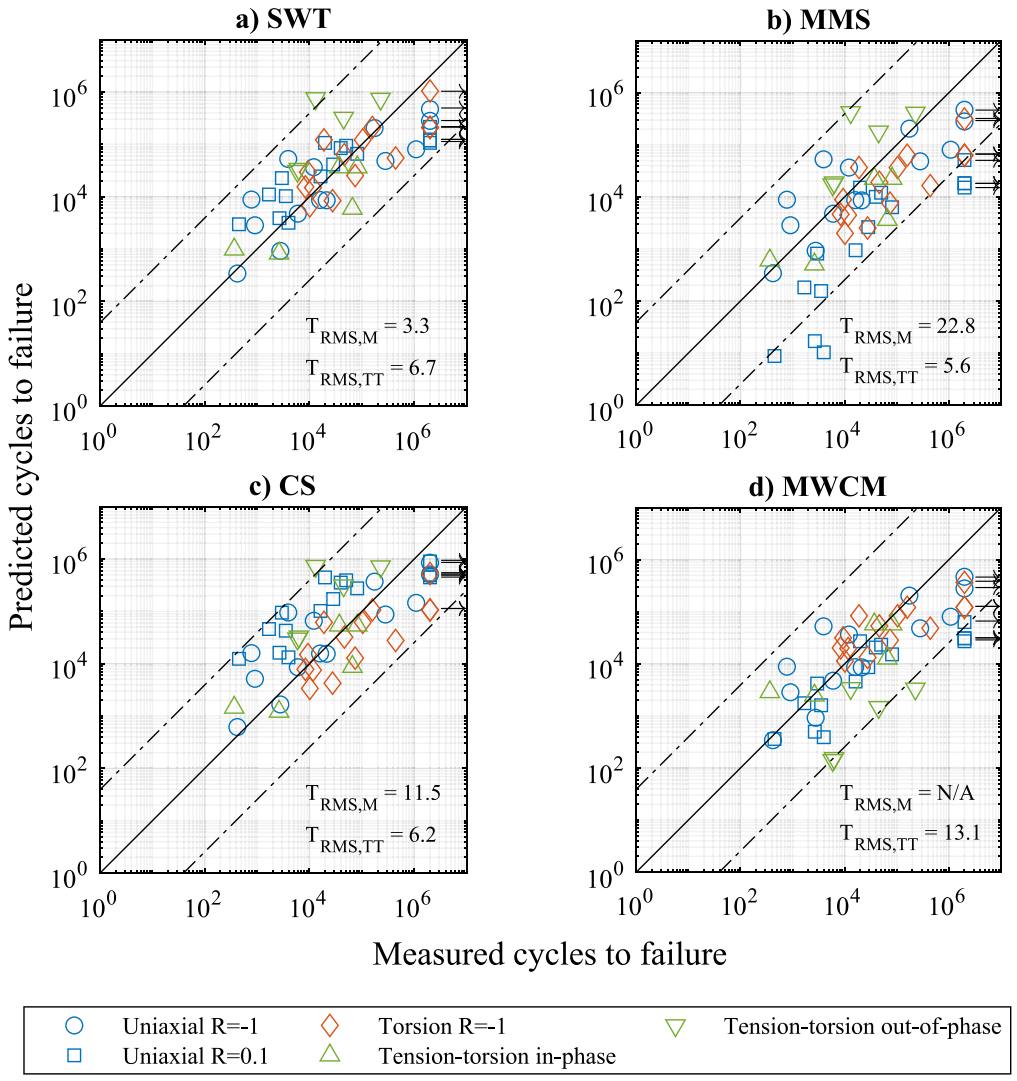

Fig. 6. Predicted cycles to failure vs measured cycles to failure for six fatigue criteria. Dashed lines show the fully reversed uniaxial scatter band.

Tovo *et al.* [27] and Benedetti *et al.* [28] were processed using the same techniques as the GCI pipe material data and the results are summarised in Table 3.

From Table 3 it is apparent that the DCIs investigated by Tovo *et al.* [27] and Benedetti *et al.* [28] demonstrated very similar fatigue behaviour for all loading conditions, with some small differences in the exact values of reference stress amplitude and slope of the fatigue curve. The fatigue response of the GCI material investigated in the present work is also similar to the DCIs for all loading types investigated, particularly when the large degree of scattering present in the BS416-2 pipe GCI fatigue data is considered. Of particular interest is that both the GCI and the DCIs show little difference in their response to proportional and non-proportional loading.

All four fatigue criteria provided reasonable predictions for the new BS416-2 fatigue data, with a small number of data points falling outside the scatter bands derived from the uniaxial $R = -1$ data. The SWT criterion (Fig. 6a) provided good predictions for all the load types investigated and received the lowest T_{RMS} score for uniaxial $R = 0.1$ loading ($T_{RMS,M} = 3.3$). This observed effectiveness of the SWT at predicting uniaxial mean stress and torsional fatigue strengths for GCI aligns with the findings of Fash and Socie [17] and Weinacht and Socie [18]. Performance of the SWT criterion for multiaxial loading ($T_{RMS,TT} = 6.7$) was slightly worse than the MMS (Fig. 6b, $T_{RMS,TT} = 5.6$) and CS (Fig. 6c, $T_{RMS,TT} = 6.2$) criteria. However, all three criteria showed similar trends for multiaxial loading in that the TTIP predictions were very good and the TTOOP loading predictions were on the non-conservative side. Both the SWT and CS criteria had one TTOOP data point that fell just outside the scatter bands.

For the SWT and MMS criteria TTOOP was the only loading condition tested where the critical planes experienced a variable shear stress because the principal stress axes rotated. The fact that these two criteria both underestimated the damage caused by this loading and both took no account of shear stresses suggests that this variable shear stress caused some damage that was not accounted for. This closely matches the finding of Tovo *et al.* [27] for DCI that the normal stress amplitude and mean on the critical plane correlated all results well, except those obtained under TTOOP loading where the experimental strength was lower than predicted.

At higher stress amplitudes the MMS criterion underestimated the fatigue life of specimens subject to uniaxial loading with a mean stress. As a result the MMS criterion received the worst T_{RMS} score for uniaxial $R = 0.1$ loading ($T_{RMS,M} = 22.8$). The overestimations of uniaxial $R = 0.1$ fatigue lives occurred for lives less than 10^4 cycles. Marquis and Karjalainen-Roikonen [32] did not report this underestimation of mean stress fatigue lives for DCI, although this could be because their data featured no results with fatigue lives less than 10^4 cycles.

The CS criterion (Fig. 6c) verged on providing non-conservative predictions for uniaxial mean stress loading ($T_{RMS,M} = 11.5$), although

no predictions fell outside the scatter bands. Unlike the MMS, this inaccuracy for the CS criterion occurred across the full range of fatigue lives.

Like the other criteria, the MWCM (Fig. 6d) predicted the cycles to failure of the TTIP data well, however, the TTOOP fatigue life predictions of the were on the conservative side, giving the MWCM the worst T_{RMS} score for multiaxial loading ($T_{RMS.TT} = 13.1$). This is because $\rho_{eff} = 1$ for both TTOOP loading with $R = -1$ and uniaxial loading with $R = -1$, so the MWCM predicted the same response for both types of loading. Fig. 4 shows that, in terms of shear stress amplitude, TTOOP loading is less damaging than uniaxial loading for this GCI.

The SWT and MMS criteria were able to make good predictions despite only using the uniaxial $R = -1$ data for calibration and using no shear stress terms. This strongly suggests that tensile cracking dominates the fatigue life of this GCI under the HCF regime, which aligns with the findings of Fash [51] and Weinacht & Socie [18] that under torsional and uniaxial loading Stage II crack growth comprised 90–95% of the fatigue life of their GCI specimens. The observed similarity of fatigue behaviour between GCI and DCI suggests that cracking processes similar to those observed by Billaudeau, Nadot and Bezine [33] for DCI may also occur in GCI. Specifically, that the crack initiates under a shearing mode at stress concentrations caused by internal defects in the material but quickly transitions to a tensile crack growth mode. The fracture surfaces of specimens failed by uniaxial, torsional, and TTIP loading also coincided with the maximum normal stress amplitude plane, as reported in Section 4, although these surfaces are more likely associated with a fast fracture process in the final cycle than the bulk of the fatigue life.

Returning to the aim of this work, all four fatigue criteria investigated were able to provide reasonable fatigue life predictions for the GCI pipe material investigated. The MMS criterion offered the best multiaxial fatigue predictions, closely followed by the CS and SWT criteria. However, both the MMS and CS criteria were unable to accurately predict the mean stress effect while the SWT criterion was able to predict this well without needing mean stress calibration data. Therefore, the SWT criterion can be considered to provide the best overall fatigue life predictions for multiaxial fatigue of water pipe GCI in the HCF regime.

7. Conclusions

The aim of this work was to identify a fatigue criterion that is able to predict the multiaxial High-Cycle Fatigue (HCF) response of water pipe (GCI). To obtain the fatigue data needed for this investigation, BS416-2 pipe material was used to represent GCI water pipe material. The conclusions drawn from this work are as follows.

- The BS416-2 pipe material displays very similar uniaxial fatigue behaviour and mean stress sensitivity to literature data for GCI water pipe material supporting the use of BS416-2 pipes as an alternative to GCI water pipes for fatigue testing.
- GCI and Ductile Cast Iron (DCI) demonstrate similar multiaxial fatigue behaviour suggesting that the findings of previous studies regarding crack initiation and growth processes in DCI may also apply to GCI. Additionally, the fact that DCI has also been used to manufacture water pipes means a single fatigue condition assessment process could be developed that covers both pipe materials.
- Of the multiaxial fatigue criteria investigated, the Smith-Watson-Topper (SWT) criterion was considered to provide the best overall predictions for the GCI pipe material investigated. The effectiveness of the SWT criterion closely aligns with previous observations that tensile crack growth dominates the fatigue life of GCI.

CRediT authorship contribution statement

Edward John: Methodology, Formal analysis, Investigation, Writing – original draft. **Joby Boxall:** Conceptualization, Writing – review & editing. **Richard Collins:** Conceptualization, Writing – review & editing, Funding acquisition. **Elisabeth Bowman:** Conceptualization, Writing – review & editing. **Luca Susmel:** Conceptualization, Methodology, Writing – review & editing, Project administration, Funding acquisition.

Declaration of Competing Interest

The authors declare that they have no known competing financial interests or personal relationships that could have appeared to influence the work reported in this paper.

Data availability

Data will be made available on request.

Acknowledgements

This work was funded by UK Water Industry Research (UKWIR) and the EPSRC through the Water Infrastructure and Resilience (WIRe) Centre for Doctoral Training. The authors would like to thank Dennis Dellow from UKWIR for bringing an experienced industry perspective to the project. Also a special thanks to the technicians Paul Blackbourne, Sam Gibson, Geoffrey Hibberd, Tesoro Monaghan, Mario Dorna, Chris Todd, and Richard Kay for their work which enabled the microscopy, tensile testing, and fatigue testing to take place. For the purpose of open access, the author has applied a creative commons attribution (CC BY) license to any author accepted manuscript versions arising.

References

[1] Barton NA, Farewell TS, Hallett SH, Acland TF. Improving pipe failure predictions: Factors effecting pipe failure in drinking water networks. Water Resour 2019;164:114926. https://doi.org/10.1016/j.watres.2019.114926.
[2] Boxall JB, O'Hagan A, Pooladsaz S, Saul AJ, Unwin DM. Estimation of burst rates in water distribution mains. In: Proceedings of the Institution of Civil Engineers: Water Management; 2007. https://doi.org/10.1680/wama.2007.160.2.73.
[3] Sanders J, Marshallsay D, Mountfort G, Fox G, Butler M. A Leakage Routemap to 2050; 2022. https://www.water.org.uk/news-item/milestone-leakage-routemap-to-revolutionise-the-reduction-of-leakage-from-pipes/ (accessed June 15, 2022).
[4] Economic Insight Ltd, Options for a sustainable approach to asset maintenance and replacement; 2022. https://www.water.org.uk/news-views-publications/publications/options-sustainable-approach-asset-maintenance-and-replacement (accessed September 11, 2023).
[5] Soltani Asadi Z, Melchers RE. Long-term external pitting and corrosion of buried cast iron water pipes. Corros Eng Sci Technol 2018;53:93–101. https://doi.org/10.1080/1478422X.2017.1400291.
[6] Rajeev P, Kodikara J, Robert D, Zeman P, Rajani B. Factors contributing to large diameter water pipe failure. In: Strategic Asset Management of Water and Wastewater Infrastructure: Leading Edge Strategic Asset Management, Sydney, Australia; 2013. http://www.criticalpipes.com/th_gallery/factors-contributing-to-large-diameter-water-pipe-failure-as-evident-from-failure-inspection/ (accessed September 11, 2023).
[7] Farrow J, Jesson D, Mulheron M, Nensi T, Smith P. Achieving zero leakage by 2050: The basic mechanisms of bursts and leakage. UK Water Industry Research; 2017.
[8] Brevis W, Susmel L, Boxall J. Investigating in-service failures of water pipes from a multiaxial notch fatigue point of view: A conceptual study. Proc Inst Mech Eng C J Mech Eng Sci 2015;229. https://doi.org/10.1177/0954406214553020.
[9] Jiang R, Rathnayaka S, Shannon B, Zhao X-L, Ji J, Kodikara J. Analysis of failure initiation in corroded cast iron pipes under cyclic loading due to formation of through-wall cracks. Eng Fail Anal 2019;103:238–48. https://doi.org/10.1016/j.engfailanal.2019.04.031.
[10] Melchers RE, Petersen RB, Wells T. Empirical models for long-term localised corrosion of cast iron pipes buried in soils. Corros Eng Sci Technol 2019;54:678–87. https://doi.org/10.1080/1478422X.2019.1658427.
[11] Rajani B, Makar J. A methodology to estimate remaining service life of grey cast iron water mains. Can J Civ Eng 2000. https://doi.org/10.1139/l00-073.
[12] UKWIR, Water Industry Information & Guidance Note: Ductile Iron Pipes and Fittings; 2006. https://www.water.org.uk/wp-content/uploads/2018/11/ign-4-21-01.pdf.
[13] Makar JM, Rajani B. Gray Cast-Iron Water Pipe Metallurgy. J Mater Civ Eng 2000. https://doi.org/10.1061/(asce)0899-1561(2000)12:3(245).
[14] Seica MV, Packer JA. Mechanical Properties and Strength of Aged Cast Iron Water Pipes. J Mater Civ Eng 2004. https://doi.org/10.1061/(asce)0899-1561(2004)16:1(69).

[15] Makar JM, McDonald SE. Mechanical Behavior of Spun-Cast Gray Iron Pipe. J Mater Civ Eng 2007;19:826–33. https://doi.org/10.1061/(ASCE)0899-1561(2007)19.
[16] ASTM International, Standard Test Method for Evaluating the Microstructure of Graphite in Iron Castings A247-19; 2019. https://doi.org/10.1520/A0247-19.
[17] Fash J, Socie DF. Fatigue behaviour and mean effects in grey cast iron. Int J Fatigue 1982. https://doi.org/10.1016/0142-1123(82)90040-8.
[18] Weinacht DJ, Socie DF. Fatigue damage accumulation in grey cast iron. Int J Fatigue 1987. https://doi.org/10.1016/0142-1123(87)90048-X.
[19] Kommers JB. The static and fatigue properties of some cast irons. Proc Am Soc Test Mater 1928;28:174–97. https://doi.org/10.1021/ie50012a019.
[20] Lampman S. Fatigue and Fracture Properties of Cast Irons. In: ASM Handbook; 1996, pp. 665–679. https://doi.org/https://doi-org.sheffield.idm.oclc.org/10.31399/asm.hb.v19.a0002399.
[21] Larson M, Jönsson L. Elastic Properties of Pipe Materials during Hydraulic Transients. J Hydraul Eng 1991;117:1317–31. https://doi.org/10.1061/(asce)0733-9429(1991)117:10(1317).
[22] Chan D, Gallage CPK, Rajeev P, Kodikara J. Field performance of in-service cast iron water reticulation pipe buried in reactive clay. Can Geotech J 2015. https://doi.org/10.1139/cgj-2014-0531.
[23] Randeniya C, Robert DJ, Li CQ, Kodikara J. Large-scale experimental evaluation of soil saturation effect on behaviour of buried pipes under operational loads. Can Geotech J 2020;57:205–20. https://doi.org/10.1139/cgj-2018-0544.
[24] Rezaei H, Ryan B, Stoianov I. Pipe failure analysis and impact of dynamic hydraulic conditions in water supply networks. Procedia Eng 2015;119:253–62. https://doi.org/10.1016/j.proeng.2015.08.883.
[25] Department for Transport, AADF Data - major and minor roads, Gov.Uk; 2020. https://roadtraffic.dft.gov.uk/downloads (accessed April 19, 2021).
[26] Jara-Arriagada C, Stoianov I. High resolution water pressure monitoring for the assessment of fatigue damage in water pipes. In: 2nd International Joint Conference on Water Distribution Systems Analysis and Control in the Water Industry, Valencia; 2022. https://doi.org/10.4995/WDSA-CCWI2022.2022.14813.
[27] Tovo R, Lazzarin P, Berto F, Cova M, Maggiolini E. Experimental investigation of the multiaxial fatigue strength of ductile cast iron. Theor Appl Fract Mech 2014;73:60–7. https://doi.org/10.1016/j.tafmec.2014.07.003.
[28] Benedetti M, Santus C, Raghavendra S, Lusuardi D, Zanini F, Carmignato S. Multiaxial plain and notch fatigue strength of thick-walled ductile cast iron EN-GJS-600-3: Combining multiaxial fatigue criteria, theory of critical distances, and defect sensitivity. Int J Fatigue 2022;156. https://doi.org/10.1016/j.ijfatigue.2021.106703.
[29] Socie DF. Multiaxial fatigue damage models. J Eng Mater Technol, Trans ASME 1987;109:293–8. https://doi.org/10.1115/1.3225980.
[30] Socie DF, Marquis GB. Multiaxial Fatigue; 1999. https://saemobilus-sae-org.sheffield.idm.oclc.org/content/R-234 (accessed July 26, 2021).
[31] Santecchia E, Hamouda AMS, Musharavati F, Zalnezhad E, Cabibbo M, El Mehtedi M, et al. A Review on Fatigue Life Prediction Methods for Metals. Adv Mater Sci Eng 2016;2016. https://doi.org/10.1155/2016/9573524.
[32] Marquis GB, Karjalainen-Roikonen P. Long-life multiaxial fatigue of a nodular graphite cast iron. Biaxial/Multiaxial Fatigue and Fracture 2003:105–22. https://doi.org/10.1016/S1566-1369(03)80007-9.
[33] Billaudeau T, Nadot Y, Bezine G. Multiaxial fatigue limit for defective materials: Mechanisms and experiments. Acta Mater 2004;52:3911–20. https://doi.org/10.1016/j.actamat.2004.05.006.
[34] Nadot Y, Mendez N, Ranganathan N, Beranger AS. Fatigue life assessment of nodular cast iron containing casting defects, Fatigue and Fracture of Engineering. Mater Struct 1999;22:289–300. https://doi.org/https://doi-org.sheffield.idm.oclc.org/10.1046/j.1460-2695.1999.00162.x.
[35] Marquis G, Socie D. Long-life torsion fatigue with normal mean stresses, Fatigue and Fracture of Engineering. Mater Struct 2000;23:293–300. https://doi.org/10.1046/j.1460-2695.2000.00291.x.
[36] Fatemi A, Shamsaei N. Multiaxial fatigue: An overview and some approximation models for life estimation. Int J Fatigue 2011;33:948–58. https://doi.org/10.1016/j.ijfatigue.2011.01.003.
[37] Smith P, Topper KN, Watson TH. A stress–strain function for the fatigue of metals. J Mater 1970;5:767–78. https://www.researchgate.net/publication/269929853_14_Smith_K_N_Watson_P_and_Topper_T_H_'A_StressStrain_Function_for_the_Fatigue_of_Metals_nl_of_Marls_1MLSA_5_4_767-778_Dee_1070.
[38] Dowling NE, Calhoun CA, Arcari A. Mean stress effects in stress-life fatigue and the Walker equation. Fatigue Fract Eng Mater Struct 2008;32:163–79. https://doi.org/10.1111/j.1460-2695.2008.01322.x.
[39] Carpinteri A, Spagnoli A. Multiaxial high-cycle fatigue criterion for hard metals. Int J Fatigue 2001;23:135–45. https://doi.org/10.1016/S0142-1123(00)00075-X.
[40] Carpinteri A, Spagnoli A, Vantadori S. Multiaxial fatigue assessment using a simplified critical plane-based criterion. Int J Fatigue 2011;33:969–76. https://doi.org/10.1016/j.ijfatigue.2011.01.004.
[41] Susmel L. Multiaxial notch fatigue: From nominal to local stress/strain quantities, 1st ed.. Cambridge: Woodhead Publishing Limited; 2009.
[42] Jesson DA, Le Page BH, Mulheron MJ, Smith PA, Wallen A, Cocks R, et al. Thermally induced strains and stresses in cast iron water distribution pipes: An experimental investigation. J Water Supply Res Technol AQUA 2010. https://doi.org/10.2166/aqua.2010.078.
[43] Mohebbi H, Jesson DA, Mulheron MJ, Smith PA. The fracture and fatigue properties of cast irons used for trunk mains in the water industry. Mater Sci Eng A 2010. https://doi.org/10.1016/j.msea.2010.05.071.
[44] British Standards Institution, Discharge and ventilating pipes and fittings, sand-cast or spun in cast iron - Part 2: Specifications for socketless systems. BS 416-2:1990; 1990. https://bsol-bsigroup-com.sheffield.idm.oclc.org/Bibliographic/BibliographicInfoData/000000000000225830.
[45] John E, Boxall J, Collins R, Bowman E, Susmel L. Investigating an alternative to exhumed grey cast iron water pipes for small-scale fatigue tests. In: 2nd International Joint Conference on Water Distribution Systems Analysis & Computing and Control in the Water Industry, Valencia, Spain; 2022.
[46] ASTM, Standard Practice for Statistical Analysis of Linear or Linearized Stress-Life (S-N) and Strain-Life (ε-N) Fatigue Data ASTM E739-10; 2015. https://doi.org/10.1520/E0739-10R15.
[47] ASTM, A guide for fatigue testing and the statistical analysis of fatigue data: STP 91, ASTM Compass; 1963. https://doi.org/10.1520/STP91A-EB.
[48] Sonsino CM. Course of SN-curves especially in the high-cycle fatigue regime with regard to component design and safety. Int J Fatigue 2007;29:2246–58. https://doi.org/10.1016/j.ijfatigue.2006.11.015.
[49] Susmel L. Multiaxial fatigue limits and material sensitivity to non-zero mean stresses normal to the critical planes, Fatigue and Fracture of Engineering. Mater Struct 2008;31:295–309. https://doi.org/10.1111/j.1460-2695.2008.01228.x.
[50] Walat K, Łagoda T. Lifetime of semi-ductile materials through the critical plane approach. Int J Fatigue 2014;67:73–7. https://doi.org/10.1016/j.ijfatigue.2013.11.019.
[51] Fash JW. FCP Report No.35 - Fatigue Crack Initiation and Growth in Gray Cast Iron, Urbana, Illinois; 1980. https://fcp.mechse.illinois.edu/fcp_report035/ (accessed August 12, 2022).